New Journal of Physics
The open-access journal for physics

Calculation of electrostatic fields using quasi-Green's functions: application to the hybrid Penning trap

J Verdú[1], S Kreim[2,5,6], K Blaum[3,4], H Kracke[2], W Quint[4], S Ulmer[2] and J Walz[2]

[1] Atominstitut der Österreichischen Universitäten, Stadionallee 2, A-1020 Vienna, Austria
[2] Institut für Physik, Johannes Gutenberg-Universität, D-55099 Mainz, Germany
[3] Max-Planck-Institut für Kernphysik, D-69117 Heidelberg, Germany
[4] Gesellschaft für Schwerionenforschung, D-64291 Darmstadt, Germany
E-mail: kreim@uni-mainz.de

New Journal of Physics **10** (2008) 103009 (23pp)
Received 18 June 2008
Published 8 October 2008
Online at http://www.njp.org/
doi:10.1088/1367-2630/10/10/103009

Abstract. Penning traps offer unique possibilities for storing, manipulating and investigating charged particles with high sensitivity and accuracy. The widespread applications of Penning traps in physics and chemistry comprise e.g. mass spectrometry, laser spectroscopy, measurements of electronic and nuclear magnetic moments, chemical sample analysis and reaction studies. We have developed a method, based on the Green's function approach, which allows for the analytical calculation of the electrostatic properties of a Penning trap with arbitrary electrodes. The ansatz features an extension of Dirichlet's problem to nontrivial geometries and leads to an analytical solution of the Laplace equation. As an example we discuss the toroidal hybrid Penning trap designed for our planned measurements of the magnetic moment of the (anti)proton. As in the case of cylindrical Penning traps, it is possible to optimize the properties of the electric trapping fields, which is mandatory for high-precision experiments with single charged particles. Of particular interest are the anharmonicity compensation, orthogonality and optimum adjustment of frequency shifts by the continuous Stern–Gerlach effect in a quantum jump

[5] Author to whom any correspondence should be addressed.
[6] This article comprises part of the PhD thesis of S Kreim.

spectrometer. The mathematical formalism developed goes beyond the mere design of novel Penning traps and has potential applications in other fields of physics and engineering.

Contents

1. Introduction

Penning traps are very suitable for precision experiments with charged particles since they provide long storage and observation times. Radial confinement is realized by a homogeneous magnetic field $\vec{B}$; axially the particles are trapped by an electrostatic field $\vec{E} \parallel \vec{B}$ in a harmonic trapping potential. Besides being able to confine a single charged particle, it is possible to detect it non-destructively with an electronic detection technique [1]. Currently, two types of Penning traps for measurements with relative uncertainties down to 10^{-13} [2] are being used: hyperbolic and cylindrical traps [3, 4]. The hyperbolic one has found a wide range of applications in mass spectrometry [5]. Cylindrical traps have been used for determining the g-factor of an electron bound in hydrogen-like carbon and oxygen [6, 7] as well as of the free electron [2, 8]. Moreover, Penning traps have been used to measure e.g. the antiproton's mass [9], masses of stable particles, atoms [10]–[12], and short-lived radioactive ions [13]–[16]. Furthermore, they

have been implemented in molecular electric dipole moment experiments [17], antihydrogen production [18, 19] or the most accurate test of the CPT symmetry in the lepton sector [20]. Such high-precision experiments depend critically on the correct design of the trap being used. Furthermore, novel kinds of Penning traps are coming into use: because of its scalability, for example, the planar Penning trap [21]–[23] offers possibilities for quantum computation with ions or electrons.

Our planned high-precision measurement of the magnetic moment of a single (anti)proton [24, 25] demands a Penning trap different from any existing one. The determination of the g-factor results from a precise measurement of the particle's cyclotron and Larmor frequencies [6, 7]. Since the latter is an internal degree of freedom, a magnetic bottle is exploited to imprint the spin state information onto an external degree of freedom, namely the axial eigenmotion of the particle. This so-called continuous Stern–Gerlach effect is used to detect the resulting frequency shift and thus the spin state non-destructively [26, 27]. Using a conventional cylindrical trap, like the one in [26], the continuous Stern–Gerlach effect would shift the axial frequency of a single (anti)proton on a relative 10^{-7} scale, making it almost impossible to detect efficiently. To this end, a novel Penning trap is introduced, which we call *the hybrid Penning trap*: a combination of electrodes of different shape, basically cylindrical end caps and correction electrodes and a toroidal or hyperbolic ring. In particular, the curved shape of a toroidal ferromagnetic ring enhances the curvature of the magnetic bottle by more than one order of magnitude compared with a cylindrical ring of similar dimensions and the same material, therefore making the resolution of the phase-sensitive Stern–Gerlach quantum jump spectrometer [28] big enough for the efficient determination of the spin state of a single (anti)proton.

In section 2, a 'quasi'-Green's function method is presented which will render the analytical calculation of a hybrid Penning trap (figure 1) possible. An analytical calculation of the entire electrostatic properties of a *toroidal hybrid Penning trap* consisting of two cylindrical end caps, two cylindrical correction electrodes and one toroidal ring (figure 3) will be presented in section 3. This trap is used to illustrate the 'quasi'-Green's function method developed in section 2. In section 4, detailed analytical expressions for the design of a toroidal hybrid Penning trap for high-precision experiments are given. Those formulae make the design of such traps considerably easier than any numerical approach. In section 5, further applications of the mathematical formalism developed to other fields of experimental physics are discussed focusing on ion-trapping technology and microwave engineering. Besides being our motivation for the measurement for the (anti)proton's g-factor, the power of this calculation technique goes beyond the design of the hybrid Penning trap and could be used in many other problems involving the Laplace equation.

2. The 'quasi'-Green's function solution to Dirichlet's problem

2.1. Definition of the hybrid Penning trap

The Green's function formalism is a well-known and powerful technique for calculating electrostatic potentials. In the case of ion traps, the electrostatic potential $\Phi(\vec{x})$ usually has to be calculated within a closed volume defined by some electrodes to which arbitrary voltages are applied. Mathematically, this problem simply corresponds to solving the Laplace equation with Dirichlet boundary conditions: if the adequate Green's function is available, the

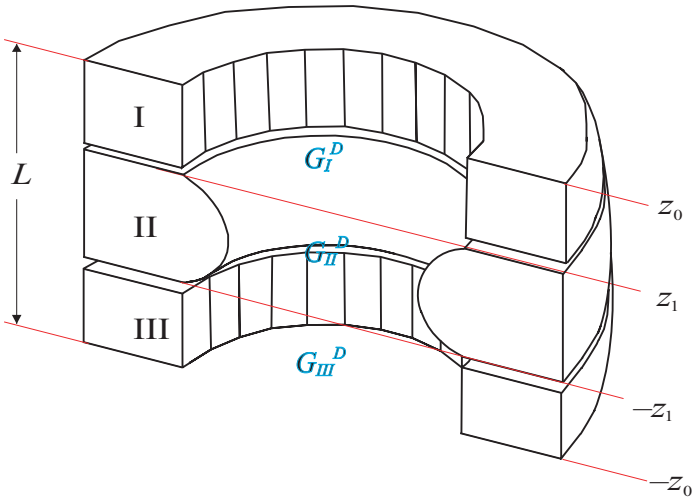

Figure 1. Inner surface of a three-pole hybrid Penning trap. The trap is made up of axially symmetric electrodes each with a different geometry. For simplicity of the figure, the upper and lower regions, Ω_{I} and Ω_{III}, respectively, are drawn to be cylindrical.

computation of $\Phi(\vec{x})$ becomes straightforward. Green's functions for electrodes with various shapes (hyperboloids, oblate and prolate spheroids, toroids, flat-ring cyclide discs, etc) are well known in the literature [29, 30]. These kinds of electrodes can be put together in many different ways, so that a vast class of well-defined trapping volumes can theoretically be envisaged with them. Any such combination of differently shaped electrodes defining a closed trapping region is what we call a *hybrid Penning trap*.

2.2. The potential problem in a hybrid Penning trap

Most hybrid traps, even if they are relatively simple like the one outlined in figure 1, do not have a known analytic expression for the Green's function fulfilling Dirichlet boundary conditions on their entire surface. If, however, for each electrode forming the trap, the corresponding Green's function, which does meet those conditions on the electrode's surface, is known, then it is possible to construct a 'quasi'-Green's function for the entire hybrid trap which delivers an analytic expression for $\Phi(\vec{x})$. The next paragraphs show formally how to construct such a 'quasi'-Green's function and how to calculate the electric potential with it. For simplicity, we will restrict the discussion to the trap sketched in figure 1, which is defined by two external cylindrical electrodes and one central ring with arbitrary but rotationally invariant surface around the $\vec{u}_z$-axis. Generalization of the presented formalism to other trapping geometries and/or to a higher number of electrodes will become apparent.

In general, the electrostatic boundary-value problem is defined by the following integral equation [31]:

$$\int_{\Omega} \mathrm{d}^3x' \left[\Phi(\vec{x}\,')\nabla'^2 G(\vec{x} \mid \vec{x}\,') - G(\vec{x} \mid \vec{x}\,')\nabla'^2\Phi(\vec{x}\,')\right] = \oint_{\partial\Omega} \mathrm{d}S' \left[\Phi(\vec{x}\,')\frac{\partial}{\partial n'} G(\vec{x} \mid \vec{x}\,') - G(\vec{x} \mid \vec{x}')\frac{\partial}{\partial n'}\Phi(\vec{x}')\right], \quad (1)$$

where Ω is the trapping volume under consideration, $\partial\Omega$ the surface delimiting that volume, and $\Phi(\vec{x}')$ the electrostatic potential. $G(\vec{x} \mid \vec{x}')$ represents the Green's function for the Laplace equation. It is symmetric with respect to interchanging the source, $\vec{x}\,'$, and field coordinates, $\vec{x}$: $G(\vec{x} \mid \vec{x}') = G(\vec{x}\,'|\vec{x})$. Further, it satisfies

$$\nabla^2 G(\vec{x} \mid \vec{x}') = \nabla'^2 G(\vec{x} \mid \vec{x}') = -4\pi\delta\left(\vec{x} - \vec{x}\,'\right); \qquad G(\vec{x} \mid \vec{x}') = \frac{1}{|\vec{x} - \vec{x}\,'|} + F(\vec{x} \mid \vec{x}'). \tag{2}$$

$F(\vec{x} \mid \vec{x}')$ represents any arbitrary function satisfying $\nabla^2 F(\vec{x} \mid \vec{x}') = \nabla'^2 F(\vec{x} \mid \vec{x}') = 0$, $\forall\{\vec{x}, \vec{x}\,'\} \in \Omega$. In the case of Dirichlet boundary conditions, $F(\vec{x} \mid \vec{x}')$ is chosen such that the Green's function becomes equal to zero at the surface of the trap: $G^{\mathrm{D}}(\vec{x} \mid \vec{x}') = 0 \ \forall \ \vec{x}\,' \in \partial\Omega$. The function $F(\vec{x} \mid \vec{x}')$ is thus a solution of the Laplace equation and it represents the potential of a (mirror) charge distribution external to the volume Ω [31]. Further, assuming the absence of free charges within the region where the potential is calculated, $\nabla^2\Phi(\vec{x}') \propto \rho(\vec{x}') = 0, \ \forall\,\vec{x}\,' \in \Omega$, equation (1) simplifies to

$$\int_\Omega \mathrm{d}^3x' \left[\Phi(\vec{x}')\nabla'^2 G^{\mathrm{D}}(\vec{x} \mid \vec{x}')\right] = \oint_{\partial\Omega} \mathrm{d}S' \left[\Phi(\vec{x}')\frac{\partial}{\partial n'} G^{\mathrm{D}}(\vec{x} \mid \vec{x}')\right]. \tag{3}$$

The validity of equation (3) is not restricted to pure Green's functions satisfying equation (2), but it applies whenever the volume Ω is free of charges and for any function being equal to zero at its surface, $G^{\mathrm{D}}(\vec{x} \mid \vec{x}') = 0\,\forall\,\vec{x}\,' \in \partial\Omega$. However, if the proper Green's function satisfying Dirichlet boundary conditions is known, then exploiting $\nabla^2 G^{\mathrm{D}}(\vec{x} \mid \vec{x}') = -4\pi\delta\,(\vec{x} - \vec{x}\,')$, equation (3) simplifies to the conventional expression $\Phi(\vec{x}) = -\frac{1}{4\pi}\oint_{\partial\Omega} \mathrm{d}S' \cdot \Phi(\vec{x}')\frac{\partial\, G^{\mathrm{D}}(\vec{x}|\vec{x}')}{\partial n'}$. The boundary conditions, $\Phi(\vec{x}')$, are provided by the applied voltages at the trap electrodes. Thus, the explicit knowledge of $G^{\mathrm{D}}(\vec{x} \mid \vec{x}')$ formally solves the potential problem, reducing it to a simple integral.

2.3. Definition of the 'quasi'-Green's function

For the hybrid trap of figure 1, we introduce a 'quasi'-Green's function, $\tilde{G}^{\mathrm{D}}(\vec{x} \mid \vec{x}')$, defined as

$$\tilde{G}^{\mathrm{D}}(\vec{x} \mid \vec{x}') = \begin{cases} G^{\mathrm{D}}_{\mathrm{I}}(\vec{x} \mid \vec{x}') & \vec{x} \in \Omega; \quad \vec{x}\,' \in \Omega_{\mathrm{I}}, \\ G^{\mathrm{D}}_{\mathrm{II}}(\vec{x} \mid \vec{x}') & \vec{x} \in \Omega; \quad \vec{x}\,' \in \Omega_{\mathrm{II}}, \\ G^{\mathrm{D}}_{\mathrm{III}}(\vec{x} \mid \vec{x}') & \vec{x} \in \Omega; \quad \vec{x}\,' \in \Omega_{\mathrm{III}}, \end{cases} \tag{4}$$

Each volume Ω_i denotes one of the i-regions into which the trapping volume of figure 1 is divided (see also figure 3). This partition of space is in principle arbitrary but must satisfy the condition that inside each Ω_i the Green's function satisfying Dirichlet boundary conditions on the physical part of that Ω_i-region (i.e. the metallic electrode) must be known. Thus, a set of functions $G^{\mathrm{D}}_i(\vec{x} \mid \vec{x}')$ must be provided satisfying $\nabla^2 G^{\mathrm{D}}_i(\vec{x} \mid \vec{x}') = \nabla'^2 G^{\mathrm{D}}_i(\vec{x} \mid \vec{x}') = 4\pi\delta(\vec{x} - \vec{x}')$ and $G^{\mathrm{D}}_i(\vec{x} \mid \vec{x}') = 0$ on the corresponding part of the trap's surface. In the example of figure 1, the partition is chosen such that there are three Ω_i-regions delimited by the 'contact' planes $z' = \pm z_1$. In principle, many different 'quasi'-Green's functions, $\tilde{G}^{\mathrm{D}}(\vec{x} \mid \vec{x}')$, can be constructed; the most convenient choice, however, depends on the actual geometry of the trap being considered.

For the 'quasi'-Green's function introduced, the interchange symmetry of the arguments is broken: $\tilde{G}^{\mathrm{D}}(\vec{x} \mid \vec{x}') \neq \tilde{G}^{\mathrm{D}}(\vec{x}\,'|\vec{x})$. Our focus is on the properties of $\tilde{G}^{\mathrm{D}}$ with respect to the source $\vec{x}\,'$. Since the constituting functions $G^{\mathrm{D}}_i(\vec{x} \mid \vec{x}')$ are chosen such that each separately

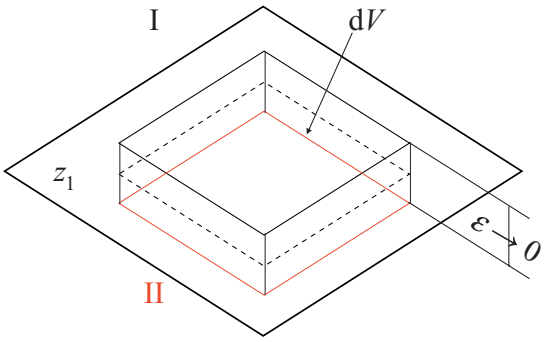

Figure 2. Illustration of the Gaussian box enclosing the point $\vec{x}\,' = \{r', \varphi', z' = +z_1\}$ which lies on the contact plane separating the regions Ω_{I} and Ω_{II}. $\tilde{G}^{\mathrm{D}}$ has a finite step discontinuity at any point on that contact plane.

satisfies Dirichlet boundary conditions for the corresponding electrode, the 'quasi'-Green's function satisfies Dirichlet boundary conditions on the entire surface of the trap: $\tilde{G}^{\mathrm{D}}(\vec{x} \mid \vec{x}') = 0$, $\forall\, \vec{x}\,' \in \partial\Omega$. As a consequence of this, equation (3) still holds and will be used in the following to calculate the potential $\Phi(\vec{x})$.

2.4. Solution with the 'quasi'-Green's function

In order to obtain $\Phi(\vec{x})$ from equation (3), the Laplacian of the 'quasi'-Green's function with respect to the source coordinates, $\nabla'^2 \tilde{G}^{\mathrm{D}}(\vec{x} \mid \vec{x}')$, has to be evaluated. For source points within the trap not lying on any of the contact planes separating the Ω_i-regions, this immediately yields: $\nabla'^2 \tilde{G}^{\mathrm{D}}(\vec{x} \mid \vec{x}') = -4\pi\delta(\vec{x} - \vec{x}')\, \forall \vec{x}\,' = \{x', y', z' \neq \pm z_1\}$, simply due to the definition of the 'quasi'-Green's function. The case of the contact surfaces has to be considered separately.

Note that $\tilde{G}^{\mathrm{D}}(\vec{x} \mid \vec{x}')$ has a finite-step discontinuity at the planes separating the Ω_i-regions, $\vec{x}\,' = \{x', y', z' = \pm z_1\}$. This discontinuity has to be taken into account when calculating the Laplacian $\nabla'^2 \tilde{G}^{\mathrm{D}}(\vec{x} \mid \vec{x}')$ at any of those points. Since ∇'^2 represents a derivative operator and since the derivative of the Heaviside step-function results in the Dirac-delta, we assume the following ansatz for $\nabla'^2 \tilde{G}^{\mathrm{D}}(\vec{x} \mid \vec{x}\,')$:

$$\nabla'^2 \tilde{G}^{\mathrm{D}}(\vec{x} \mid \vec{x}') = -4\pi\delta(\vec{x} - \vec{x}') + \delta(z' - z_1) f_+(\vec{x} \mid \vec{x}') + \delta(z' + z_1) f_-(\vec{x} \mid \vec{x}'). \quad (5)$$

With this ansatz, the Laplacian of the 'quasi'-Green's function for points not lying on the contact planes, $z' \neq \pm z_1$, is trivially recovered. The functions $f_\pm(\vec{x} \mid \vec{x}\,')$ still have to be determined.

It is obvious from equation (5) that it suffices to evaluate $f_\pm$ for points lying on the contact planes; in cylindrical coordinates: $\vec{x}\,' = \{r', \varphi', z' = \pm z_1\}$ for $f_\pm$, respectively. On the one hand, consider an infinitesimal volume $\mathrm{d}V$ enclosing the point of interest $\{r', \varphi', z' = z_1\}$ as shown in figure 2. The divergence theorem applied to $\tilde{G}^{\mathrm{D}}(\vec{x} \mid \vec{x}')$ at $\mathrm{d}V$ states that

$$\int_{\mathrm{d}V} \mathrm{d}^3x' \cdot \nabla'^2 \tilde{G}^{\mathrm{D}}(\vec{x} \mid \vec{x}') = \oint_S \mathrm{d}\vec{S}\,' \cdot \nabla' \tilde{G}^{\mathrm{D}}(\vec{x} \mid \vec{x}')\,. \quad (6)$$

In the limit $\epsilon \to 0$, the lateral surface of the Gaussian box does not contribute to the surface integral in equation (6), thus $\oint_S \mathrm{d}\vec{S}\,' \cdot \nabla' \tilde{G}^{\mathrm{D}}(\vec{x} \mid \vec{x}') = \oint_{S_\perp} \mathrm{d}S'_z \frac{\partial}{\partial z'} \tilde{G}^{\mathrm{D}}(\vec{x} \mid \vec{x}')$. The top and bottom surfaces of the Gaussian box of figure 2 are denoted by $S_\perp$; only these contribute to the

surface integral. The integral on the top surface is performed while $z' = z_1 + \epsilon \Rightarrow z' \in \Omega_{\mathrm{I}}$ and $\tilde{G}^{\mathrm{D}}(\vec{x} \mid \vec{x}') = G^{\mathrm{D}}_{\mathrm{I}}(\vec{x} \mid \vec{x}')$. For the bottom plane, $z' = z_1 - \epsilon$ and $\tilde{G}^{\mathrm{D}}(\vec{x} \mid \vec{x}') = G^{\mathrm{D}}_{\mathrm{II}}(\vec{x} \mid \vec{x}')$. Further, $\mathrm{d}S'_z$ has the opposite orientation in the latter case as compared with the former, hence leading to

$$\oint_S \mathrm{d}\vec{S}' \cdot \nabla' \tilde{G}^{\mathrm{D}}(\vec{x} \mid \vec{x}') = \lim_{\epsilon \to 0} \oint_{S_\perp} \mathrm{d}S'_z \frac{\partial}{\partial z'} \left[G^{\mathrm{D}}_{\mathrm{I}}(\vec{x} \mid r', \varphi', z_1 + \epsilon) - G^{\mathrm{D}}_{\mathrm{II}}(\vec{x} \mid r', \varphi', z_1 - \epsilon) \right]. \tag{7}$$

On the other hand, with the ansatz of equation (5) and assuming that $\vec{x} \neq \vec{x}\,'$ (thus $\vec{x}$ is outside of $\mathrm{d}V$), the volume integral in equation (6) yields

$$\int_{\mathrm{d}V} \mathrm{d}^3x' \cdot \nabla'^2 \tilde{G}^{\mathrm{D}}(\vec{x} \mid \vec{x}') = \int_{\mathrm{d}V} \mathrm{d}z' \cdot \mathrm{d}S'_z \, \delta(z - z_1) f_+(\vec{x} \mid r', \varphi', z') = \int_{S_\perp} \mathrm{d}S'_z \, f_+(\vec{x} \mid r', \varphi', z_1). \tag{8}$$

Now, we can obtain the explicit form of f_+ by comparing equation (7) with (8). Taking into account that $G^{\mathrm{D}}_i(\vec{x} \mid \vec{x}') = \frac{1}{|\vec{x} - \vec{x}\,'|} + F^{\mathrm{D}}_{\mathrm{i}}(\vec{x} \mid \vec{x}')$, while taking the limit $\epsilon \to 0$ in equation (7), results in:

$$f_+(\vec{x} \mid r', \varphi', z_1) = \frac{\partial}{\partial z'} \left[F^{\mathrm{D}}_{\mathrm{I}}(\vec{x} \mid r', \varphi', z_1) - F^{\mathrm{D}}_{\mathrm{II}}(\vec{x} \mid r', \varphi', z_1) \right]. \tag{9}$$

The same considerations carried out for the contact plane between regions Ω_{II} and Ω_{III} deliver the function f_-:

$$f_-(\vec{x} \mid r', \varphi', -z_1) = \frac{\partial}{\partial z'} \left[F^{\mathrm{D}}_{\mathrm{II}}(\vec{x} \mid r', \varphi', -z_1) - F^{\mathrm{D}}_{\mathrm{III}}(\vec{x} \mid r', \varphi', -z_1) \right]. \tag{10}$$

Finally, computing the integral of equation (3) and resolving for $\Phi(\vec{x})$, we obtain the electrostatic potential inside the trap:

$$\begin{aligned} \Phi(\vec{x}) = &-\frac{1}{4\pi} \oint_{\partial\Omega} \mathrm{d}S' \, \Phi(\vec{x}') \frac{\partial}{\partial n'} \tilde{G}^{\mathrm{D}}(\vec{x} \mid \vec{x}') \\ &+ \frac{1}{2} \int_0^{R_0} \mathrm{d}r' r' \, \Phi(r', z_1) \frac{\partial}{\partial z'} \left[F^{\mathrm{D}}_{\mathrm{I}}(\vec{x} \mid r', z_1) - F^{\mathrm{D}}_{\mathrm{II}}(\vec{x} \mid r', z_1) \right] \\ &+ \frac{1}{2} \int_0^{R_0} \mathrm{d}r' r' \, \Phi(r', -z_1) \frac{\partial}{\partial z'} \left[F^{\mathrm{D}}_{\mathrm{II}}(\vec{x} \mid r', -z_1) - F^{\mathrm{D}}_{\mathrm{III}}(\vec{x} \mid r', -z_1) \right]. \end{aligned} \tag{11}$$

In equation (11), R_0 represents the radius of the contact surface delimiting the different Ω_i-regions. Note that the integral over φ' has been assumed to deliver the value 2π in the last two summands of equation (11). This assumption is valid only if the electrostatic potential is axially symmetric. If this is not the case, those summands become surface integrals and the integration over $\varphi' \in [0, 2\pi]$ still has to be performed. In the usual case of the trap having point symmetry with respect to its central plane $z = 0$, the function f_- becomes identical to f_+ except for the negative sign. The opposite sign results from the opposite direction of the surface vector $\mathrm{d}\vec{S}'$ when calculating the integral on the right-hand side of equation (6). Taking this symmetry into account the calculation of the electrostatic potential simplifies to

$$\begin{aligned} \Phi(\vec{x}) = &-\frac{1}{4\pi} \oint_{\partial\Omega} \mathrm{d}S' \, \Phi(\vec{x}') \cdot \frac{\partial}{\partial n'} \tilde{G}^{\mathrm{D}}(\vec{x} \mid \vec{x}') \\ &+ \int_0^{R_0} r' \mathrm{d}r' \, \Phi(r', z_1) \cdot \frac{\partial}{\partial z'} \left[F^{\mathrm{D}}_{\mathrm{I}}(\vec{x} \mid r', z_1) - F^{\mathrm{D}}_{\mathrm{II}}(\vec{x} \mid r', z_1) \right]. \end{aligned} \tag{12}$$

2.5. Properties of the solution

Equation (12), or more generally equation (11), represents the formal solution of the boundary-value problem defined by the stack of electrodes of figure 1. With explicit knowledge of $F_i^{\mathrm{D}}(\vec{x} \mid \vec{x}')$, the electrostatic potential inside the trapping volume can be obtained by integration of equation (12). The main features of equation (12) are as follows.

1. It represents an integral equation: the potential $\Phi(\vec{x})$ appears not only as the pre-specified boundary conditions on the trap's surface but also in the second integral over the contact planes where $\Phi(\vec{x})$ is *a priori* unknown.
2. The first integral in equation (12) represents the zeroth-order approximation to the potential, $\Phi_0(\vec{x})$. It is the linear superposition of the potentials created individually by each electrode with the corresponding voltage. However, $\Phi_0(\vec{x})$ does not fulfill the boundary conditions on the surface of the entire trap. Upon putting the electrodes together to form the trap, the superficial charges induced by each electrode on all others arrange in such a way that the final electric potential, $\Phi(\vec{x})$, fulfills the boundary conditions on the entire trap's surface. The influence of these mutually induced charges on the final potential $\Phi(\vec{x})$ is given by the second integral in equation (12) denoted by $\Delta\Phi(\vec{x})$. The mathematical expression for the process described is an integral equation: $\Phi(\vec{x}) = \Phi_0(\vec{x}) + \Delta\Phi(\vec{x})$.
3. If all electrodes have the same shape, the functions F_i^D become the same $F_{\mathrm{I}}^{\mathrm{D}} = F_{\mathrm{II}}^{\mathrm{D}} = F_{\mathrm{III}}^{\mathrm{D}}$ and hence $\tilde{G}^{\mathrm{D}}$ simplifies to the usual Green's function. Furthermore, equation (12) reduces to the well-known expression of the electrostatic potential for the simple Dirichlet's problem.

In principle, equations (12) and (11) may be applied to many different problems. Their generalization to situations where axial symmetry is broken and/or where the shape of the electrodes is non-cylindrical is straightforward as long as a 'quasi'-Green's function as introduced in equation (4) can be constructed. In order to illustrate the power of the presented method, the complete calculation of the *toroidal hybrid trap* is performed with the help of equation (12) in the next section. The properties of such a trap will be discussed in detail in section 4. Other possible applications of equation (12) will be briefly presented in section 5.

3. Application of the method: the toroidal hybrid trap

As an example of the formalism presented, we calculate the electrostatic potential within a Penning trap formed by a toroidal ring of circular cross section and cylindrical correction electrodes and end caps, which fits exactly in the kind of hybrid trap considered in the previous section and outlined in figure 1. The toroidal hybrid trap is sketched in detail in figures 3 and 4. Applying equation (12) to the toroidal hybrid trap is straightforward; the first step consists of constructing the appropriate 'quasi'-Green's function.

3.1. Construction of an appropriate 'quasi'-Green's function

The basic Green's function for the Laplace equation, $\frac{1}{|\vec{x}-\vec{x}'|}$, has been calculated in cylindrical coordinates elsewhere [29, 31, 32]. A simple modification of that basic function leads to the Green's function inside a cylindrical box satisfying Dirichlet boundary conditions, employing

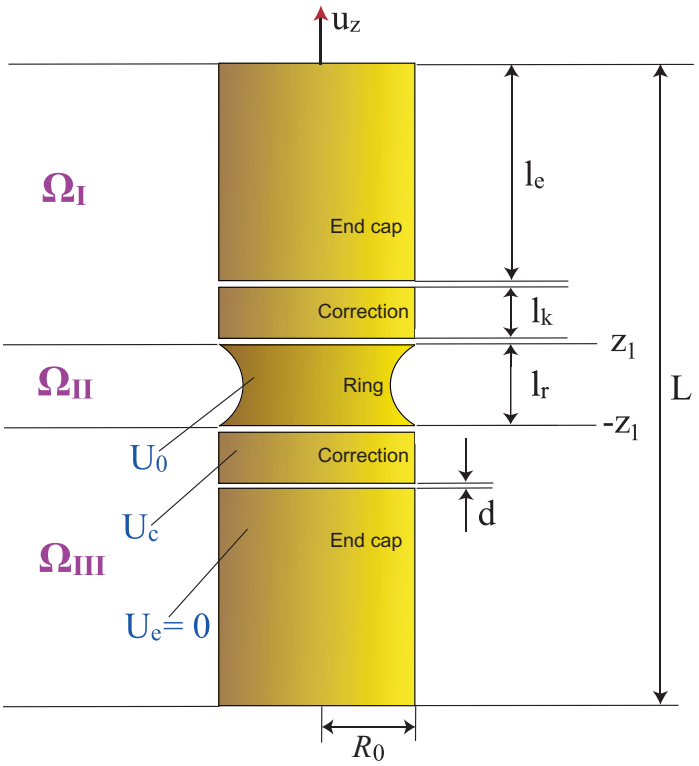

Figure 3. Inner surface of a hybrid Penning trap with toroidal ring electrode and cylindrical correction electrodes and end caps. Region I includes the upper correction electrode and end cap, region II includes the toroidal ring, and region III the lower correction and end cap electrode.

the coordinate system of figure 3:

$$G_{\mathrm{cyl}}(r, z \mid r', z') = \frac{4}{L} \sum_{n=1,3,\ldots}^{\infty} \cos(\kappa_n z) \cos(\kappa_n z') \frac{I_0(\kappa_n r_<)}{I_0(\kappa_n R_0)} \Big[I_0(\kappa_n R_0) K_0(\kappa_n r_>) - I_0(\kappa_n r_>) K_0(\kappa_n R_0) \Big]. \tag{13}$$

Here, $\kappa_n = n\pi/L$ with L being the total length of the trap given by $L = 4\,d + 2\,l_{\mathrm{e}} + 2\,l_{\mathrm{k}} + l_{\mathrm{r}}$. The notation $r_{>(<)}$ means the bigger (smaller) of (r, r'). The different letters denote the lengths of the different electrodes as shown in figure 3: l_{e} = length of the end cap, l_{k} = length of the correction electrode, l_{r} = length of the ring ($l_{\mathrm{r}} = 2z_1$), and d = the small gap between electrodes. The inner radius of the electrodes is given by R_0, which coincides with the parameter R_0 defined in section 2. The symbols I_0 and K_0 represent the modified Bessel functions of zeroth order, first and second kind, respectively. In equation (13) we have assumed axial symmetry (rotational invariance around $\vec{u}_z$); hence the azimuth angle φ does not appear. Further, we have assumed the electric potential to be point-symmetric with respect to the trap's center ($z = 0$); thus only $\cos(\kappa_n z)$-functions appear in the series.

For equation (13) to be strictly valid, the trap should be closed by a grounded disc on each side allowing for the basic Green's function in cylindrical coordinates to be simplified to a series with the summation index κ_n running over odd n only in contrast to an integral form with continuous summation index κ. Usually, the traps used in experiments are not closed

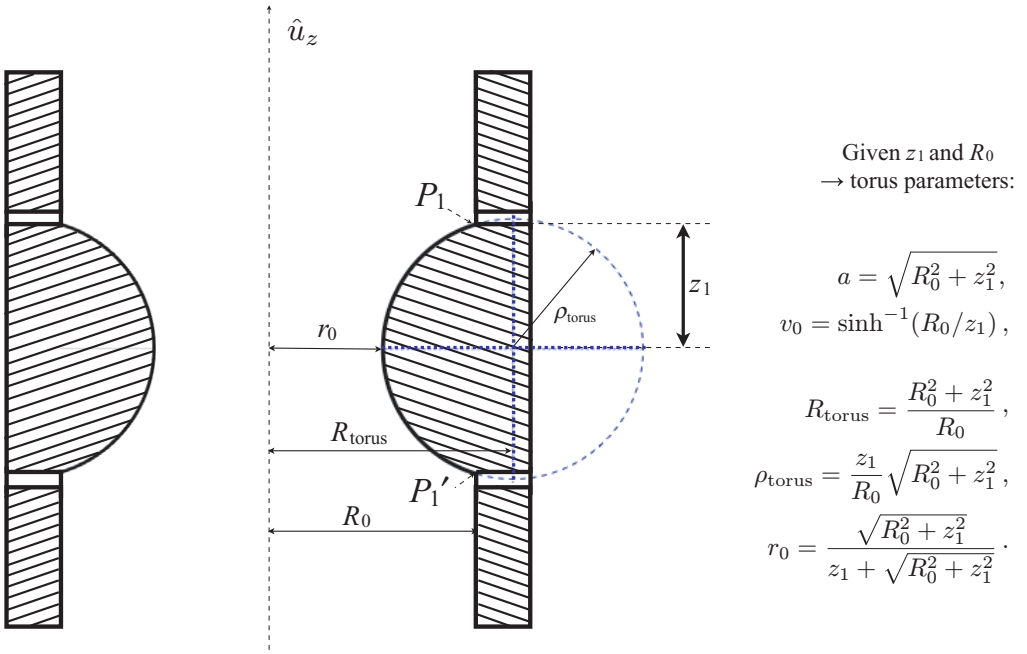

Figure 4. Parameters of the toroidal ring. The outer radius of the torus R_{torus} does not necessarily coincide with the inner radius of the cylindrical electrodes, R_0. This is reflected by the (arbitrarily chosen) upper and lower cut-off planes of the torus at P_1 and P_1', respectively: in this example, below the actual north and south poles of the torus.

by such grounded discs. This issue has been investigated mathematically in [33]: an end cap three times longer than the inner radius suffices for minimizing deviations (below 1%) of the trap's electrical properties calculated with equation (13) compared with those calculated with an infinitely long open end cap. In addition, the measurement of the electronic g-factor on carbon and oxygen [6, 7] has shown deviations as low as one part in a million in the experimental values of the coefficients c_2, c_4 and d_2 [34] from the theoretical predictions of equation (13) (see section 4). In this latter case, the measurements have been performed with a cylindrical trap with $l_e \simeq 2R_0$. For the toroidal hybrid trap a similar or even better accuracy can be assumed due to the enhanced shielding of the trap's center from outside by the toroidal ring.

The basic Green's function in toroidal coordinates has also been calculated elsewhere [29, 32, 35]. With it, the Green's function satisfying Dirichlet boundary conditions on the surface of a torus with circular cross section can be obtained employing standard techniques [31]; the result is:

$$G_{\text{tor}}(u, v \mid u', v') = \frac{1}{a\,\pi}\sqrt{\cosh v - \cos u}\,\sqrt{\cosh v' - \cos u'}\cdot\sum_{m=0}^{\infty}\epsilon_m\,\cos(mu)\cos(mu')$$
$$\times\frac{P_{m-(1/2)}(\cos v_<)}{P_{m-1/2}(\cosh v_0)}\cdot\big(P_{m-(1/2)}(\cosh v_0)\,Q_{m-(1/2)}(\cosh v_>)$$
$$-P_{m-(1/2)}(\cosh v_>)\,Q_{m-(1/2)}(\cosh v_0)\big)\,. \qquad (14)$$

$P_{m-(1/2)}$ and $Q_{m-(1/2)}$ denote the Legendre functions of first and second kind, respectively. For the case discussed here with $m \in \mathbb{N}$, they are also known as *toroidal functions* [29, 36]. The Neumann factor [29] is given by $\epsilon_m = 2 - \delta_{m,0}$. The toroidal coordinates $\{u, v, \varphi\}$ relate to the Cartesian coordinates via: $\{x, y, z\} = a/(\cosh v - \cos u)\,\{\cos\varphi \sinh v, \sin\varphi \sinh v, \sin u\}$ [29, 35]. In this coordinate system, a toroidal ring is defined by $v = v_0$, with $v_0 = \text{constant} > 0$, $u \in [0, 2\pi]$ and $\varphi \in [0, 2\pi]$. The notation $v_{>(<)}$ in equation (14) again means the bigger (smaller) of (v, v'). As before, axial symmetry is assumed and hence the azimuth φ does not appear in equation (14). Moreover, the electric potential is assumed to be invariant across the equatorial plane of the torus; thus only $\cos(mu)$—but no $\sin(mu)$—functions appear in equation (14).

For further calculation, we set the upper and lower points of the torus *looking into* the inner trap's surface as the points P_1 and P_1', respectively (see figure 4). In toroidal coordinates they are given by: $P_1 \equiv (u = \pi/2, v_0, \varphi)$ and $P_1' \equiv (u = 3\pi/2, v_0, \varphi)$. The choice of P_1 and P_1' is completely arbitrary; the reason for that specific choice is purely technical: since they are localized slightly below the ring's north and south poles, more of the correction electrodes is seen from the trap's center, and thus shielding due to the toroidal ring is reduced. An additional free parameter is the length of the ring seen from the inner side of the trap, $l_r = 2z_1$. Having specified z_1, P_1, P_1' and R_0, the toroidal ring is completely defined yielding the toroidal parameters: $a = \sqrt{R_0^2 + z_1^2}$ and $v_0 = \sinh^{-1}(R_0/z_1)$.

3.2. Potential of the toroidal hybrid trap in zeroth-order approximation

With the geometry of figure 3 chosen, it is obvious that $G_{\mathrm{I}}^{\mathrm{D}}(\vec{x} \mid \vec{x}') = G_{\mathrm{III}}^{D}(\vec{x} \mid \vec{x}') \equiv G_{\mathrm{cyl}}(\vec{x} \mid \vec{x}')$ and $G_{\mathrm{II}}^{\mathrm{D}}(\vec{x} \mid \vec{x}') \equiv G_{\mathrm{tor}}(\vec{x} \mid \vec{x}')$. Using Abel's identity, the Wronskian of the Bessel functions of equation (13) is evaluated to [36]: $I(x)\frac{\mathrm{d}K(x)}{\mathrm{d}x} - \frac{\mathrm{d}I(x)}{\mathrm{d}x}K(x) = \frac{1}{x}$ and similarly for the toroidal functions of equation (14): $P(x)\frac{\mathrm{d}Q(x)}{\mathrm{d}x} - \frac{\mathrm{d}P(x)}{\mathrm{d}x}Q(x) = \frac{1}{x}$. With these Wronskian determinants, the derivative $\partial\tilde{G}^{\mathrm{D}}(\vec{x}, \vec{x}')/\partial n'$ on the trap's surface is greatly simplified. Using the boundary conditions of figure 3, the electric potential $\Phi_0(\vec{x}) = \Phi_{\mathrm{cyc}}(\vec{x}) + \Phi_{\mathrm{tor}}(\vec{x})$ is obtained:

$$\begin{aligned}
\Phi_{\mathrm{cyl}}(r, z) &= -\frac{1}{4\pi}\int_0^{2\pi} R_0\,\mathrm{d}\varphi' \cdot 2\int_{z_1}^{L/2} \mathrm{d}z'\,\Phi(R_0, z') \cdot \left.\frac{\partial\, G_{\mathrm{cyl}}(r, z \mid r', z')}{\partial r'}\right|_{r'=R_0} \\
&= \frac{2}{L}\sum_{n=1,3,\ldots}^{\infty} \frac{1}{I_0(\kappa_n R_0)}\left[2\int_{z_1}^{L/2} \mathrm{d}z'\,\Phi(R_0, z')\cos(\kappa_n z')\right] I_0(\kappa_n r)\cdot\cos(\kappa_n z) \\
\Phi_{\mathrm{tor}}(u, v) &= -\frac{1}{4\pi}\int_0^{2\pi} h_{\varphi'}\cdot\mathrm{d}\varphi' \int_{\pi/2}^{3\pi/2} h_{u'}\cdot\mathrm{d}u'\,\Phi(v_0, u')\frac{1}{h_{v'}}\left.\frac{\partial\, G_{\mathrm{tor}}(u, v \mid u', v')}{\partial v'}\right|_{v'=v_0} \\
&= \frac{U_0}{2\pi}\sqrt{\cosh v - \cos u}\sum_{m=0,1,\ldots}^{\infty}\epsilon_m \frac{\left[\int_{\pi/2}^{3\pi/2}\mathrm{d}u' \dfrac{\cos(mu')}{\sqrt{\cosh v_0 - \cos u'}}\right]}{P_{m-(1/2)}(\cosh v_0)} P_{m-(1/2)}(\cosh v)\cdot\cos(m\,u).
\end{aligned} \tag{15}$$

The factor of 2 appearing in front of the integral $\int_{z_1}^{L/2}\mathrm{d}z'$ arises from the symmetry of the trap around the $z = 0$ plane. In the case where the voltages applied to lower correction electrode and/or end cap differ from those applied to the corresponding upper electrodes, a further integral $\int_{-L/2}^{-z_1}\mathrm{d}z'$ would have to be evaluated instead. The scale factors of the toroidal coordinates, $h_{u'}$

and $h_{v'}$, are equal [35] and in the expression for calculating Φ_{tor} they just simplify. On the other hand, the scale factor $h_{\varphi'} = \frac{a \sinh v_0}{\cos u' - \cosh v_0}$ has to be included in the integral. Furthermore, it has been assumed that the ring has a constant voltage $U_0 \rightarrow \Phi(u', v_0) = U_0\,, \forall\, u' \in [0, 2\pi]$. As mentioned before, the latter integral $\int_{P_1}^{P_1'} \mathrm{d}u'$ is delimited to the surface 'looking' inside the trap's volume. Finally, the toroidal coordinates (u, v) can be transformed into the cylindrical ones (r, z). The transformation is given by $v = 2\,\mathrm{Re}[\coth^{-1}(\frac{r+\mathrm{i}z}{a})]$ and $u = -2\,\mathrm{Im}[\coth^{-1}(\frac{r+\mathrm{i}z}{a})]$ [35].

3.3. *The electric potential of the toroidal hybrid trap*

Having obtained the zeroth-order approximation $\Phi_0(r, z)$, we are now in a position to solve the integral equation:

$$\Phi(r,z) = \Phi_0(r,z) + \int_0^{R_0} \mathrm{d}r'\, r'\, \Phi(r', z_1) \underbrace{\left[\frac{\partial F_{\text{cyl}}(r, z \mid r', z_1)}{\partial z'} - \frac{\partial F_{\text{tor}}(r, z \mid r', z_1)}{\partial z'}\right]}_{f_+(r,z|r',z_1)}. \tag{16}$$

The explicit forms of the functions $F_{\text{cyl}}(r, z|r', z')$ and $F_{\text{tor}}(r, z|r', z')$ result from the corresponding Green's functions from equations (13) and (14), as defined in equation (2):

$$\begin{aligned} F_{\text{cyl}}(r, z \mid r', z') &= -\frac{4}{L} \sum_{n=1,3,\ldots}^{\infty} \frac{K_0(\kappa_n R_0)}{I_0(\kappa_n R_0)} \cos(\kappa_n z) \cos(\kappa_n z')\, I_0(\kappa_n r) I_0(\kappa_n r') \\ F_{\text{tor}}(u, v \mid u', v') &= -\frac{1}{a\pi} \sqrt{\cosh v - \cos u}\, \sqrt{\cosh v' - \cos u'} \\ &\quad \times \sum_{m=0}^{\infty} \epsilon_m \frac{Q_{m-(1/2)}(\cosh v_0)}{P_{m-(1/2)}(\cosh v_0)} \cdot \cos(mu) \cos(mu') \cdot P_{m-(1/2)}(\cosh v)\, P_{m-(1/2)}(\cosh v'). \end{aligned} \tag{17}$$

The structure of the integral equation (16) itself already suggests the solution: the zeroth-order approximation $\Phi_0(r, z)$ has to be substituted into the integral on the right-hand side of equation (16) to get the first-order correction: $\Delta\Phi_1(r, z) = \int_0^{R_0} \mathrm{d}r'\, r'\, \Phi_0(r', z_1)\, f_+(r, z \mid r', z_1)$, which leads to the first-order approximation $\Phi_1(r, z) = \Phi_0(r, z) + \Delta\Phi_1(r, z)$. The complete solution of the integral equation is obtained by iteration: $\Phi(r, z) = \lim_{j\rightarrow\infty} \Phi_j(r, z)$, where $\Phi_j(r, z)$ denotes the jth-order approximation to the potential given by:

$$\Phi_j(r,z) = \Phi_0(r,z) + \underbrace{\int_0^{R_0} \mathrm{d}r'\, r'\, \Phi_{j-1}(r', z_1)\, f_+(r, z \mid r', z_1)}_{\Delta\Phi_j(r,z)}. \tag{18}$$

The zeroth-order approximation of the potential $\Phi_0(r, z)$ consists of linear combinations of the sets of functions $\{I_0(\kappa_n r) \cdot \cos(\kappa_n z)\}$ and $\{P_{m-(12)}(\cosh v) \cdot \cos(m u)\}$ as can be seen from equation (15). These sets both form a basis of the linear space including the solutions to the Laplace equation in the appropriate coordinate systems. Additionally, the propagator $f_+(r, z|r', z_1)$ from equation (17) also consists of a linear combination of $\{I_0(\kappa_n r) \cdot \cos(\kappa_n z)\}$ and $\{P_{m-(12)}(\cosh v) \cdot \cos(m u)\}$. Hence, the corrections $\Delta\Phi_j(r, z)$ can be written as linear

combinations of these sets, and the electric potential can be expanded as follows:

$$\Phi(r,z) = U_0 \sum_{n=1,3\ldots}^{\infty} A_n\, I_0(\kappa_n r)\cdot\cos(\kappa_n z) + U_0\sqrt{\cosh v - \cos u}\sum_{m=0,1,2,\ldots}^{\infty} B_m\, P_{m-(1/2)}(\cosh v)\cdot\cos(mu). \tag{19}$$

In order to obtain an explicit form of the potential $\Phi(r,z)$, the coefficients A_n and B_m have to be determined iteratively following the scheme presented above. Therefore, the expansion coefficients of the jth iteration of the potential $\Phi_j(r,z)$ are given by $A_n^{(j)}$ and $B_m^{(j)}$. According to equation (19) their value is related to the coefficients of the zeroth-order approximation through the correction terms $\Delta A_n^{(j)}$ and $\Delta B_m^{(j)}$ such that: $A_n^{(j)} = A_n^{(0)} + \Delta A_n^{(j)}$ and $B_m^{(j)} = B_m^{(0)} + \Delta B_m^{(j)}$. The zeroth-order approximation of the expansion coefficients can be taken from equation (15). The correction terms of the jth order are obtained by substituting $\Phi_{j-1}(r,z)$ in equation (18). Resolving for the expansion coefficients yields, with the boundary conditions taken from figure 3,

$$A_n^{(0)} = \frac{8}{L\cdot d\cdot\kappa_n^2\, I_0(\kappa_n R_0)}\left[\sin\left(\frac{\kappa_n(d+2z_1)}{2}\right)\sin\left(\frac{\kappa_n d}{2}\right) - \frac{\kappa_n d}{2}\sin(\kappa_n z_1) + 2\,T\sin\left(\frac{\kappa_n(d+l_k)}{2}\right)\cos\left(\frac{\kappa_n(2d+2z_1+l_k)}{2}\right)\sin\left(\frac{\kappa_n d}{2}\right)\right];\quad n=1,3,5,\ldots,$$

$$B_m^{(0)} = \frac{1}{2\pi}\,\frac{\epsilon_m}{P_{m-(1/2)}(\cosh v_0)}\int_{\pi/2}^{3\pi/2} \mathrm{d}u\,\frac{\cos(mu)}{\sqrt{\cosh v_0 - \cos u}};\quad m=0,1,2,\ldots, \tag{20}$$

In equation (20) the tuning ratio is defined as: $T = U_c/U_0$. The potential at the isolating gaps between neighboring electrodes has been approximated by a linear interpolation of the constant voltages applied at those electrodes. This approximation is valid whenever those gaps are small compared with the lengths of the trap's electrodes.

The jth-order correction terms of the expansion coefficients are given by

$$\Delta A_n^{(j)} = \frac{1}{U_0}\,\alpha_n\int_0^{R_0}\mathrm{d}r\, r\,\Phi_{j-1}(r,z_1)\,I_0(\kappa_n r);\quad \alpha_n = \frac{4\kappa_n}{L}\,\frac{K_0(\kappa_n R_0)}{I_0(\kappa_n R_0)}\,\sin(\kappa_n z_1),$$
$$\Delta B_m^{(j)} = \frac{1}{U_0}\,\beta_m\int_0^{R_0}\mathrm{d}r\, r\,\Phi_{j-1}(r,z_1)\,\mathrm{Y}_m(r,z_1);\quad \beta_m = \frac{\epsilon_m}{4\pi a^2}\,\frac{Q_{m-(1/2)}(\cosh v_0)}{P_{m-(1/2)}(\cosh v_0)}. \tag{21}$$

The iteration order j obviously starts at $j=1$ and should theoretically go up to infinity. The function $Y_m(r,z)$ is given by $Y_m(r,z) = \sqrt{\cosh v - \cos u}\,\{(4m-2)\cos(mu)P_{m-(3/2)}(\cosh v)\sin u + 4m\,P_{m-(1/2)}(\cosh v)\,[\sin(mu) - \cosh v\,\sin((m+1)u)]\}$, which results from the derivation of the Green's function of the torus $\partial F_{\mathrm{tor}}(r,z|r',z_1)/\partial z'$ as indicated in equation (16). In the expression for $Y_m(r,z)$ the toroidal coordinates (u,v) must be transformed into the cylindrical ones (r,z_1).

If for each new iteration the integrals in equation (21) had to be evaluated, the process of calculating the correction coefficients would be extremely cumbersome. Fortunately, this is not the case: equation (21) shows that the correction terms $\Delta A_n^{(j)}$, $\Delta B_m^{(j)}$ are related to the

expansion coefficients $A_n^{(j-1)}$, $B_m^{(j-1)}$ through a simple linear relation, enabling us to write in matrix notation:

$$\begin{pmatrix} \Delta A_p^{(j)} \\ \Delta B_q^{(j)} \end{pmatrix} = \begin{pmatrix} S_{p,n} & T_{p,m} \\ V_{q,n} & W_{q,m} \end{pmatrix} \cdot \begin{pmatrix} A_n^{(j-1)} \\ B_m^{(j-1)} \end{pmatrix}; \quad \mathcal{U} = \begin{pmatrix} S_{p,n} & T_{p,m} \\ V_{q,n} & W_{q,m} \end{pmatrix}. \tag{22}$$

The matrices for the correction terms and expansion coefficient are column vectors of dimension $(N+M)\times 1$, where N and M denote the number of terms used in the expansion of the cylindrical and toroidal part of $\Phi(r,z)$, respectively, as can be seen from equation (19). Theoretically, an exact solution demands $N, M \to +\infty$. Moreover, the $(N+M)\times(N+M)$ square matrix $\mathcal{U}$ depends only on the geometry of the hybrid trap: $\mathcal{U} = \mathcal{U}(L, R_0, z_1)$. It depends neither on the iteration order j nor on the applied voltages U_0, U_c. Its elements are integrals which need to be evaluated once. The explicit form of $\mathcal{U}$ is obtained after some tedious algebraic calculations; here we just present the result:

$$\begin{aligned}
S_{p,n} &= \alpha_p \cos(\kappa_n z_1) \cdot \begin{cases} n = p & \frac{1}{2} R_0^2 \left[I_0 (\kappa_n R_0)^2 - I_1 (\kappa_n R_0)^2 \right], \\ n \neq p & \dfrac{R_0}{\kappa_p^2 - \kappa_n^2} \left[\kappa_p I_0(\kappa_n R_0) I_1(\kappa_p R_0) - \kappa_n I_0(\kappa_p R_0) I_1(\kappa_n R_0) \right] \end{cases} \\
T_{p,m} &= \alpha_p \cdot \int_0^{R_0} \mathrm{d}r\, r\, I_0(\kappa_p r) \sqrt{\cosh v - \cos u}\, P_{m-(1/2)}(\cosh v) \cos(mu), \\
V_{q,n} &= \beta_q \cos(\kappa_n z_1) \cdot \int_0^{R_0} \mathrm{d}r\, r\, Y_q(r, z_1) I_0(\kappa_n r), \\
W_{q,m} &= \beta_q \cdot \int_0^{R_0} \mathrm{d}r\, r\, Y_q(r, z_1) \sqrt{\cosh v - \cos u}\, P_{m-(1/2)}(\cosh v) \cos(mu).
\end{aligned} \tag{23}$$

In general, the sub-matrices of $\mathcal{U}$ each have a different dimension: $S \equiv N \times N$, $T \equiv N \times M$, $V \equiv M \times N$ and $W \equiv M \times M$. The expansion coefficients A_n, B_n of the potential are thus given by

$$\begin{pmatrix} A_n \\ B_m \end{pmatrix} = \sum_{j=0}^{\infty} \mathcal{U}^j \cdot \begin{pmatrix} A_n^{(0)} \\ B_m^{(0)} \end{pmatrix}. \tag{24}$$

Now, the iteration coefficient j starts from $j = 0$ since the zeroth-order coefficients $A_n^{(0)}$, $B_m^{(0)}$ have to be included in the above summation. Technically, the matrix $\mathcal{U}$ together with the initial zeroth-order coefficients $A_n^{(0)}$, $B_m^{(0)}$ delivers the solution of the potential $\Phi(r,z)$ inside the toroidal hybrid trap.

3.4. Comments on the solution

The main features of the solution for the hybrid trap obtained in the preceding section are the following:

1. The solution is analytical; the function $\Phi(r,z)$ is obtained as given in equation (19). However, the coefficients A_n, B_m will be in general numerical, with no closed symbolic expression. The analyticity of $\Phi(r,z)$ has decisive advantages over a pure numerical approach when designing the trap. This will become clear in section 4.

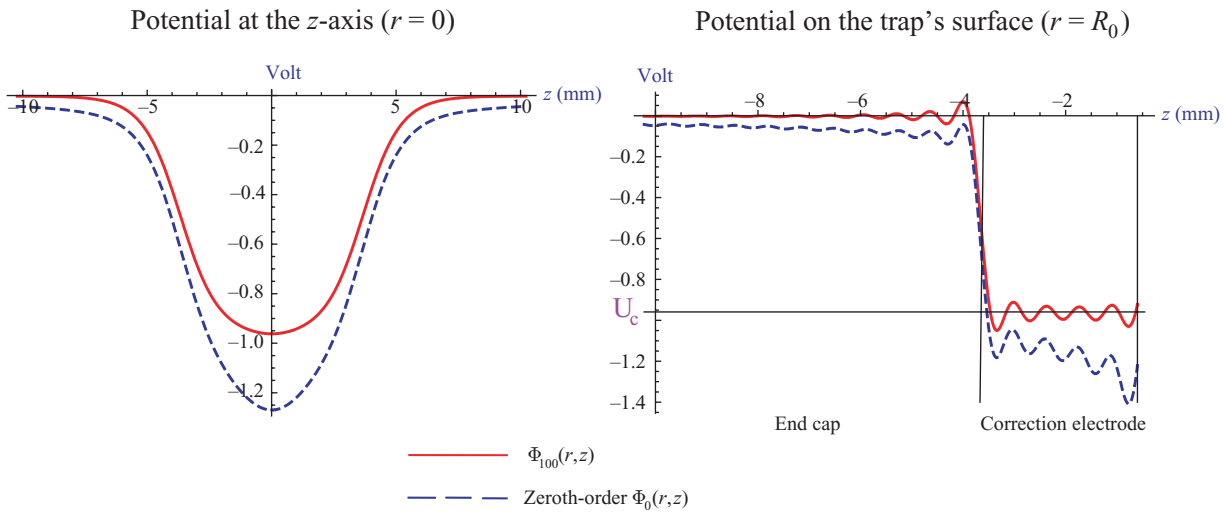

Figure 5. Example of the potential of a toroidal hybrid trap. The ring voltage is set to $U_0 = -1\,\mathrm{V}$ with a tuning ratio of $T = 0.96$ and grounded end caps. The roughness of the zeroth-order approximation $\Phi_0(r, z)$ is visible: the boundary conditions are not fulfilled, neither at the correction electrode nor at the end cap. On the contrary, the 'exact solution' $\Phi_{100}(r, z)$ fulfills them. All graphs are calculated with $R_0 = 2\,\mathrm{mm}$, $z_1 = 0.46\,\mathrm{mm}$, $L = 20.44\,\mathrm{mm}$ and $N = M = 40$.

2. $\Phi(r, z)$ is a linear combination of functions obeying the Laplace equation; therefore it itself satisfies $\nabla^2\Phi(r, z) = 0$ inside the trapping volume. A plot of $\Phi(r, z)$ on the surface of the trap showing that it also satisfies the boundary conditions confirms *ex post* its validity. This is demonstrated in figures 5 and 6.
3. An exact calculation of the potential would theoretically require infinite terms and summands. In practice though, we observe that setting $N = M = 20$ suffices for calculating the potential close to the $\hat{u}_z$-axis, which is usually the region of interest.
4. The main difficulty in the calculation is the computation of $\mathcal{U}$, which requires $(N + M)^2$ numerical integrations. The complexity of the problem increases quadratically with the number of terms N, M.

3.5. *Convergence of the iterative solution*

The convergence of equation (24) is guaranteed by the fact that $\lim_{j\to\infty} \mathcal{U}^j = 0$. This can be proved for any geometrical parameters L, R_0, z_1 and exploiting that $\lim_{j\to\infty} \alpha_n^j = \lim_{j\to\infty} \beta_m^j = 0\,\forall\, n, m$. Convergence is provided by the fact that $K_0^j(\kappa_n R_0)$ and $Q_{m-1/2}^j(\cosh v_0)$ tend very rapidly to zero for increasing j and n, m, respectively. Upon exponentiating, any element of the matrix $\mathcal{U}_{n,m}^j$ contains products of the form $\alpha_n^k \cdot \beta_m^l$ with $k + l \leqslant j$ which tend to zero while $k, l \to \infty$; therefore $\lim_{j\to\infty} \mathcal{U}_{n,m}^j = 0$ holds. In figure 7, the convergence of the particular $\mathcal{U}^j$ for the example considered in figures 5 and 6 is shown.

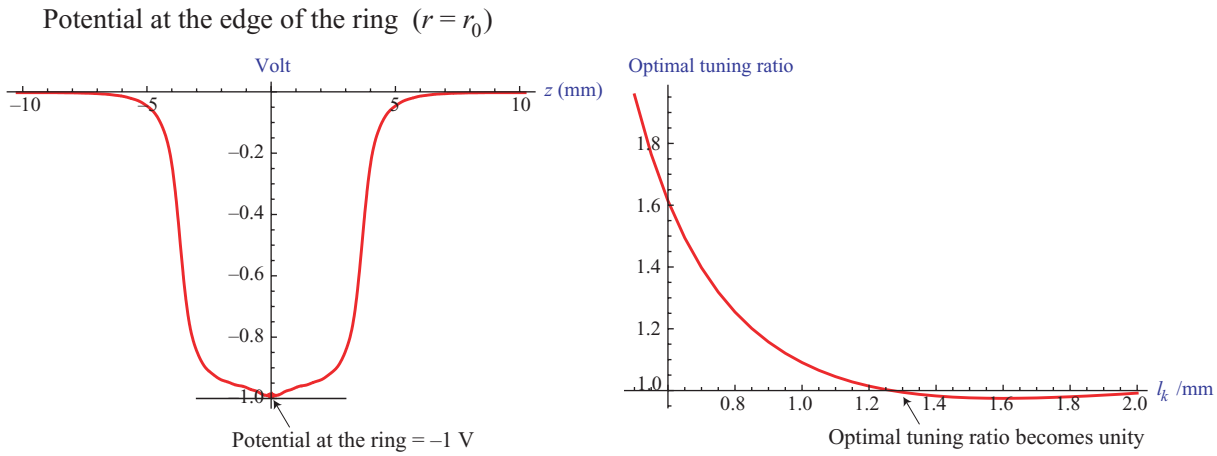

Figure 6. Left: the curve shows that the boundary conditions are fulfilled at the ring. Right: optimal tuning ratio as a function of the length of the correction electrode. For one specific length, $l_k = 1.25$, the optimal tuning ratio can even be set to 1.

3.6. The electric potential of the cylindrical Penning trap

As a corollary of the calculation of $\Phi_0(r, z)$ in the previous section, the potential of the cylindrical Penning trap is obtained by adding a further integral of the form $\int_{-z_1}^{z_1} \mathrm{d}z'\, U_0 \cos(\kappa_n z')$ to $\Phi_{\mathrm{cyl}}(r, z)$ from equation (13), where U_0 is the applied voltage to the (cylindrical) ring. With the boundary conditions shown in figure 3, the potential of the cylindrical Penning trap is given by:

$$\Phi_{\mathrm{cylinder}}(r, z) = U_0 \sum_{n=1,3,\ldots}^{\infty} \left\{ \frac{8}{L \cdot d \cdot {\kappa_n}^2 \cdot I_0(\kappa_n R_0)} \sin\left(\frac{\kappa_n d}{2}\right) \left[\sin\left(\frac{\kappa_n (d + l_r)}{2}\right) + 2\, T \sin\left(\frac{\kappa_n (d + l_k)}{2}\right) \cos\left(\frac{\kappa_n (2d + l_r + l_k)}{2}\right) \right] I_0(\kappa_n r) \cdot \cos(\kappa_n z) \right\}. \tag{25}$$

Here, $l_r = 2\, z_1$ is now the length of the cylindrical ring. All electrostatic properties of the cylindrical five-electrode Penning trap can be deduced from equation (25). Of special relevance for precision experiments are *compensation* and *orthogonality*, which will be investigated for the toroidal hybrid trap in section 4.

3.7. The electric potential of a toroidal ring

As in the case of the cylindrical trap, the electric potential created by a ring of circular cross section at a constant voltage is obtained as a corollary of the calculation of $\Phi_0(r, z)$ for the toroidal hybrid trap. Taking into account that $\int_0^{2\pi} \mathrm{d}u' \frac{\cos(mu')}{\sqrt{\cosh v_0 - \cos u'}} = 2\sqrt{2}\, Q_{m-(1/2)}(\cosh v_0)$ [29, 37], we have

$$\Phi_{\mathrm{torus}}(u, v) = U_0 \frac{\sqrt{2}}{\pi} \sqrt{\cosh v - \cos u} \sum_{m=0,1,\ldots}^{\infty} \epsilon_m \frac{Q_{m-(1/2)}(\cosh v_0)}{P_{m-(1/2)}(\cosh v_0)} P_{m-(1/2)}(\cosh v) \cdot \cos(mu). \tag{26}$$

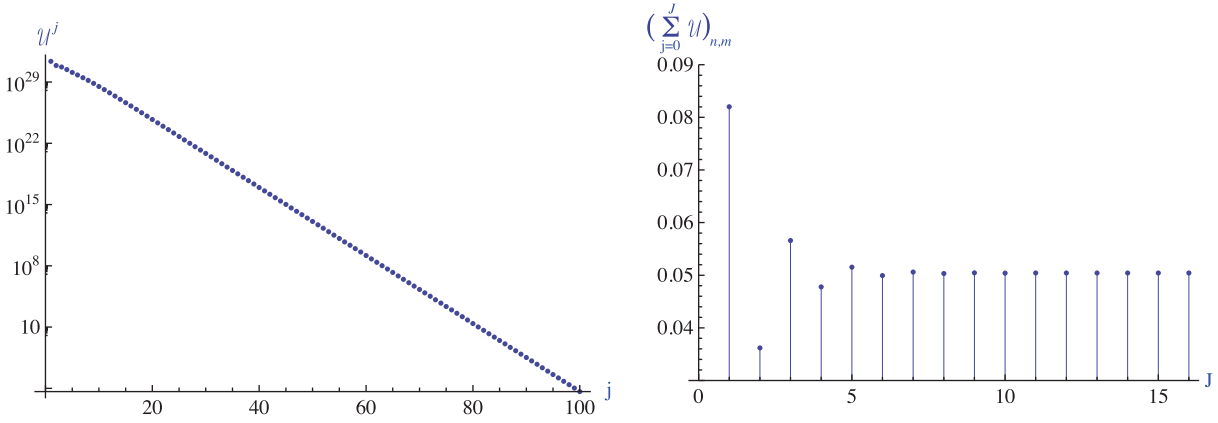

Figure 7. Example of the convergence of $\sum_{j=0}^{\infty}\mathcal{U}^j$. The semilogarithmic plot on the left shows how the norm of the $\mathcal{U}$ vanishes with increasing exponent: $|\,\mathcal{U}^j\,| \to 0$. The graph on the right shows the convergence of an arbitrary element of $\sum_{j=0}^{\infty}\mathcal{U}^j$ after having added a few summands to the series. All elements of that matrix satisfy this behavior.

This expression is valid for points outside the torus. It can be converted to Cartesian (x, y, z) or cylindrical coordinates (r, φ, z) with the transformations given in sections 3.1 and 3.2, respectively.

4. Anharmonicity compensation and orthogonality of the toroidal hybrid trap

Precision experiments with ion traps depend critically on the electrostatic performance of the trap. For example, the compensation of electrostatic anharmonicities of a Penning trap was first achieved by *Dehmelt* [38] in the context of his famous $g-2$ experiment [4]. The so-called c_j- and d_j-*coefficients* determine systematically the electrostatic properties of any Penning trap and are essential for its accurate design. These coefficients have been extensively investigated for both truncated hyperbolic [39] and cylindrical traps [3]. Their meaning and relevance for high-precision Penning trap experiments is also described in [40]. In this section, we will derive analytic expressions for c_j- and d_j-coefficients for the toroidal hybrid trap. This will clearly illustrate the power of the method developed in section 3. The task of designing a suitable toroidal hybrid trap for high-precision experiments, like the planned measurement of the g-factor of the (anti)proton, is enormously simplified having analytic expressions for the fundamental coefficients c_2, c_4, c_6 and d_2. Higher-order coefficients can also be calculated without any additional numerical effort.

4.1. Determination of c_2, c_4 and c_6 for the toroidal hybrid trap

Close to the center of the trap ($r = z = 0$) the electrostatic potential of equation (19) can be expressed as a Taylor expansion of the form:

$$\Phi(r,z) = \Phi_0 + r\,\frac{\partial\Phi}{\partial r} + z\,\frac{\partial\Phi}{\partial z} + \frac{r^2}{2!}\,\frac{\partial^2\Phi}{\partial r^2} + \frac{z^2}{2!}\,\frac{\partial^2\Phi}{\partial z^2} + \cdots = \sum_{j=0}^{\infty}\sum_{i=0}^{j}\binom{j}{i}\,\frac{\partial^j\Phi}{\partial r^i\,\partial z^{j-i}}\,r^i z^{j-i}, \qquad (27)$$

where all derivatives are evaluated at $r = z = 0$. We define the c_j-coefficients as

$$c_j = \frac{1}{U_0} \cdot \frac{1}{j!} \cdot \frac{\partial^j \Phi(r, z)}{\partial z^j}\bigg|_{(0,0)}. \tag{28}$$

These coefficients are solely functions of the trap geometry and the applied tuning ratio: $c_j = c_j(l_e, l_k, l_r, d, R_0, T)$. From equation (19) the determination of c_j is straightforward through direct derivation. The first most relevant ones are given by

$$\begin{aligned}
c_2 &= -\frac{1}{2}\left(\sum_{n=1,3,\ldots}^{\infty} A_n \kappa_n^2 + \frac{\sqrt{2}}{a^2}\sum_{m=0,1,\ldots}^{\infty} B_m(-1)^m(4m^2+1)\right),\\
c_4 &= \frac{1}{24}\left(\sum_{n=1,3,\ldots}^{\infty} A_n \kappa_n^4 + \frac{\sqrt{2}}{a^4}\sum_{m=0,1,\ldots}^{\infty} B_m(-1)^m(16m^4+56m^2+9)\right),\\
c_6 &= \frac{1}{720}\left(\sum_{n=1,3,\ldots}^{\infty} A_n \kappa_n^6 + \frac{\sqrt{2}}{a^6}\sum_{m=0,1,\ldots}^{\infty} B_m(-1)^m(64m^6+512m^4+1756m^2+225)\right).
\end{aligned} \tag{29}$$

Note that due to the symmetry of the potential across $z = 0$, all odd coefficients vanish. Thus, with the coefficients A_n and B_m of equation (24) already computed, the c_j-coefficients can be found without loss of accuracy.

4.2. Optimal tuning ratio and orthogonality

The c_j-coefficients can be written as the sum of two terms: $c_j = e_j(l_e, l_k, l_r, d, a) + T \cdot d_j(l_e, l_k, l_r, d, a)$, which can be seen from equation (20). If the applied tuning ratio $T = U_c/U_0$ is chosen such that $T = -e_4/d_4$, then c_4 is automatically canceled. The biggest electric anharmonicity is normally represented by that coefficient. With $c_4 = 0$ the trap is said to be *compensated* and $T = -e_4/d_4$ is the *optimal tuning ratio*. Compensation is absolutely necessary for many high-precision experiments since, as a result, the frequency of the trapped particle does not depend on its oscillation amplitude. Thus, uncontrolled or systematic errors are substantially reduced and the frequency can be treated as a constant for many applications. The specific optimal tuning ratio for the toroidal hybrid trap in the example of figure 5 can be taken from figure 8 after having computed c_4 with equation (29) for different values of T.

An additional property usually desired in precision Penning traps is the *orthogonality* [3]. A trap is said to be *orthogonal* when the curvature of the trapping potential is independent of the applied tuning ratio: $c_2 \neq c_2(T)$ or $d_2 = \frac{\partial c_2}{\partial T} = 0$. As before, the d_2-coefficient is received from equation (29) through derivation:

$$d_2 = -\frac{1}{2}\left(\sum_{n=1,3,\ldots}^{\infty} \frac{\partial A_n}{\partial T}\kappa_n^2 + \frac{\sqrt{2}}{a^2}\sum_{m=0,1,\ldots}^{\infty} \frac{\partial B_m}{\partial T}(-1)^m(4m^2+1)\right). \tag{30}$$

To compute $\frac{\partial A_n}{\partial T}$, $\frac{\partial B_m}{\partial T}$, the zeroth-order coefficients $A_n^{(0)}$, $B_m^{(0)}$ from equation (20) first have to be derived and, subsequently, equation (24) is used to achieve the desired level of precision.

In figure 8, d_2 has been calculated as a function of the length of the correction electrode l_k, while keeping all other geometric parameters constant. It can be seen that for one specific l_k the d_2-coefficient is equal to zero and the trap of the example becomes orthogonal.

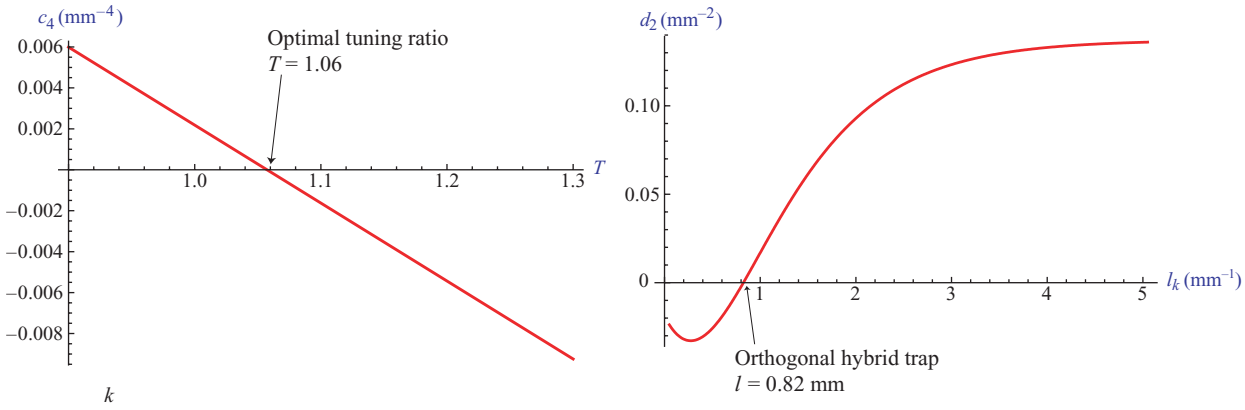

Figure 8. Left: the c_4 term can be canceled by applying the optimal tuning ratio. Right: a specific l_k makes $d_2 = 0$ and the trap becomes orthogonal.

Table 1. Parameters of an orthogonalized and compensated *toroidal hybrid trap*.

Geometric and electrical properties			
R_0	3.600 mm	d_2	4.02797×10^{-5} mm^{-2}
z_1	0.200 mm	T_{c_4}	0.913088
l_k	1.279 mm	$c_4(T_{c_4})$	-2.51735×10^{-8} mm^{-4}
l_e	8.741 mm	$c_6(T_{c_4})$	-3.43197×10^{-5} mm^{-6}

4.3. Numerical example for an orthogonal and compensated toroidal hybrid trap

Table 1 shows a numerical example for an orthogonal and compensated toroidal hybrid trap. To achieve this, the trap is first made orthogonal for a specific thickness of the ring l_r via the corresponding length of the correction electrode l_k. Subsequently, the coefficient c_4 is tuned to zero with the appropriate tuning ratio. Finally, the value of the coefficient c_6 is determined. Since machining of the parts sets a limit of some micrometres to the accuracy achievable, the coefficients will never be identical to zero. As a measure of how well the trap is orthogonalized, it is therefore convenient to examine the change of axial frequency ν_z as a function of the tuning ratio. With the calculated d_2-coefficient of $d_2 = 4.02797 \times 10^{-5}\,\mathrm{mm}^{-2}$, a micro-unit change in the tuning ratio shifts ν_z by 0.1 mHz at an axial frequency in the case of a singly trapped proton of roughly 700 kHz, which is negligible.

Thus, we have demonstrated that the parameters of the toroidal hybrid trap can be tuned in such a way as to yield a harmonic potential and an orthogonal trap, where the axial frequency depends neither on the axial energy nor the voltage applied to the correction electrode. Finally, the hybrid traps offer all the tuning possibilities for which cylindrical Penning traps are exploited.

5. Further applications

The calculation of the toroidal hybrid trap for the measurement of the g-factor of the (anti)proton [24, 25] has been the main motivation for the general method developed in

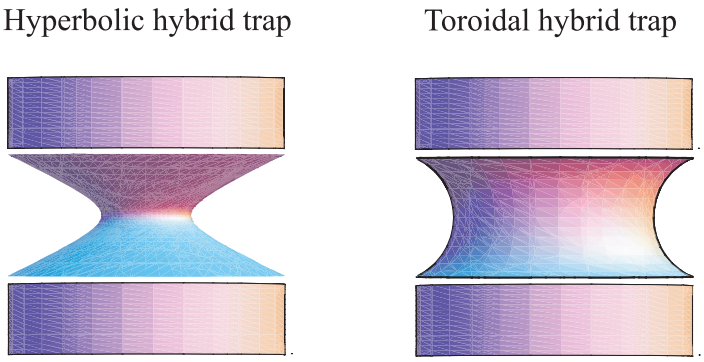

Figure 9. The hyperbolic hybrid trap is an interesting possibility which can be calculated analytically with the 'quasi'-Green's function method of section 3.

section 2. Beyond that, the method can solve the Laplace equation analytically in many other situations. Here, we want to comment briefly on some possibilities.

5.1. Other possible hybrid traps

Different hybrid traps can be thought of just by replacing the toroidal ring by other electrodes with more convenient shapes depending on the goal of the experiments. For example, in high-precision mass measurements with experimental setups at room temperature, like those of [15, 41], traditional hyperbolic Penning traps are commonly used. This is due to the larger volume in which the potential is harmonic as compared with cylindrical traps. However, no analytic formulae have been known for these traps until now. A hyperbolic hybrid trap with a (truncated) hyperbolic ring and cylindrical correction electrodes and end caps would have a very similar harmonicity volume plus the advantages of being open, and therefore easily accessible for beam-lines. Moreover, it would be much easier to design with the method of section 2 and easier to machine. The basic Green's function $\frac{1}{|\vec{x}-\vec{x}'|}$ is well known in oblate spheroidal coordinates [29, 30, 32], with which the 'quasi'-Green's function for the hyperbolic hybrid trap can be constructed, and hence application of equation (12) becomes straightforward. A comparison between the hyperbolic and toroidal hybrid trap is shown in figure 9.

Additionally, with the method employed for the toroidal trap, an appropriate 'quasi'-Green's function for the classical hyperbolic trap (hyperbolic ring and end caps) might be constructed using oblate spheroidal coordinates; with it an analytical solution to that trap might be obtained.

5.2. Applications to planar traps

Another interesting problem that can immediately be solved with the 'quasi'-Green's function method of section 2 is the propagation of microwaves in quasi-TEM modes [42] in planar structures like micro strips, coplanar waveguides and slot lines. For instance, coplanar waveguides (short CPW) have been used recently for building planar cavities in circuit-QED experiments [43]. Experiments where the electromagnetic field of a CPW cavity is coupled to ions, neutral atoms [44] or even polar molecules [45, 46] have been proposed or are under construction. The problem of calculating the propagating quasi-TEM modes arises through the

different dielectric constant (ϵ) of the substrate and the 'air side' of the transmission line [47]. This can be easily overcome just by partitioning the space into two regions with different Green's functions, each with the corresponding ϵ and again applying equation (12). With the Green's function in rectangular Cartesian coordinates, the problem can in principle be solved easily. It must be mentioned that analytical solutions for the micro strip, CPW and slot lines have been found already [47]–[49]. However, extensions to situations with multiple substrates, partial filling with other dielectrica, etc can be handled conveniently with the 'quasi'-Green's function method of section 2 while being inaccessible by other means.

6. Conclusion

Within this article, we have presented an analytically solvable extension of Dirichlet's problem. The analytical calculation of the electric potential distribution of a novel kind of Penning trap, *the hybrid trap*, has been performed. The hybrid Penning trap introduced represents a new powerful tool in high-precision experiments. Intricate mass and g-factor measurements, such as our planned measurement of the (anti)proton's magnetic moment, appear feasible by using this novel type of trap. As mentioned before, in order to make use of the continuous Stern–Gerlach effect, a strong magnetic bottle with a high curvature B_2 is required. The magnetic bottle is superimposed onto the homogeneous magnetic field B_0 needed for radial confinement yielding a net magnetic field along $\vec{u}_z$ of the form: $B_z = B_0 + B_2 z^2$. For our measurement of the (anti)proton's magnetic moment, we have manufactured a toroidal hybrid trap with $B_2 \sim 400\,\mathrm{mT\,mm^{-2}}$, resulting in a frequency shift of about 200 mHz for a single (anti)proton at ~ 700 kHz axial frequency, thus enabling the non-destructive detection of the (anti)proton's spin state [28]. This has been our main motivation for developing the hybrid Penning trap. A complete discussion on all the advantages of this toroidal trap over other conventional designs with hyperbolic or cylindrical traps for the measurement of the (anti)proton's magnetic moment goes beyond the scope of this paper and will be reviewed in future publications.

Another type of hybrid trap can be realized by replacing the center ring by a hyperboloid, as seen in figure 9. The hyperbolic hybrid Penning trap is an attractive alternative to classical hyperbolic traps with truncated electrodes. Avoiding the difficult manufacturing process of the hyperbolic end caps and correction electrodes used in pure hyperbolic Penning traps is only one of the advantages of the hybrid hyperbolic trap worth mentioning. Additional advantages are the open access for particle injection and the good anharmonicity behavior. Furthermore, other shapes can be thought of, with which hybrid traps could increase the range of applications of Penning traps in experimental physics.

Finally, the 'quasi'-Green's function formalism developed can be extended to other problems of interest in physics and engineering. Future experiments with planar traps using microwave guides might profit from this technique.

Acknowledgments

We acknowledge funding from the Helmholtz Foundation under contract number VH-NG-037 as well as the German Science Foundation under contract number QU 122/3-1. JV acknowledges support from the Marie Curie fellowship MIEDFAM. We thank S Stahl and M Kretzschmar for fruitful discussions.

References

[1] Dehmelt H G and Walls F L 1968 Bolometric technique for the rf spectroscopy of stored ions *Phys. Rev. Lett.* **21** 127–31

[2] Hanneke D, Fogwell S and Gabrielse G 2008 New measurement of the electron magnetic moment and the fine structure constant *Phys. Rev. Lett.* **100** 120801

[3] Gabrielse G and MacKintosh F C 1984 Cylindrical Penning traps with orthogonalized anharmonicity compensation *Int. J. Mass Spectrom. Ion Process.* **57** 1

[4] Dehmelt H G 1990 Experiments with an isolated subatomic particle at rest *Rev. Mod. Phys.* **62** 525

[5] Blaum K 2006 High-accuracy mass spectrometry with stored ions *Phys. Rep.* **425** 1–78

[6] Häffner H, Beier T, Hermanspahn N, Kluge H-J, Quint W, Stahl S, Verdú J and Werth G 2000 High-accuracy measurement of the magnetic moment anomaly of the electron bound in hydrogenlike carbon *Phys. Rev. Lett.* **85** 5308–11

[7] Verdú J, Djekić S, Stahl S, Valenzuela T, Vogel M, Werth G, Beier T, Kluge H-J and Quint W 2004 Electronic g factor of hydrogenlike oxygen $^{16}O^{7+}$ *Phys. Rev. Lett.* **92** 093002

[8] Gabrielse G, Hanneke D, Kinoshita T, Nio M and Odom B 2006 New value of the fine structure constant from the electron g-value and QED *Phys. Rev. Lett.* **97** 030802

[9] Gabrielse G, Khabbaz A, Hall D S, Heimann C, Kalinowsky H and Jhe W 1999 Precision mass spectroscopy of the antiproton and proton using simultaneously trapped particles *Phys. Rev. Lett.* **82** 3198–201

[10] Pinegar D B, Zafonte S L and Van Dyck R S 2007 The UW-PTMS: recent measurements and technological progress *Hyperfine Interact.* **174** 47–53

[11] Rainville S, Thompson J K and Pritchard D E 2004 An ion balance for ultra-high-precision atomic mass measurements *Science* **303** 334–8

[12] Nagy S, Fritioff T, Suhonen M, Schuch R, Blaum K, Björkhage M and Bergström I 2006 New mass value for ^{7}Li *Phys. Rev. Lett.* **96** 163004

[13] Blaum K, Audi G, Beck D, Bollen G, Herfurth F, Kellerbauer A, Kluge H-J, Sauvan E and Schwarz S 2003 Masses of ^{32}Ar and ^{33}Ar for fundamental tests *Phys. Rev. Lett.* **91** 260801

[14] Rodríguez D *et al* 2004 Mass measurement on the rp-process waiting point ^{72}Kr *Phys. Rev. Lett.* **93** 161104

[15] Bollen G *et al* 2006 Experiments with thermalized rare isotope beams from projectile fragmentation: a precision mass measurement of the superallowed β emitter ^{38}Ca *Phys. Rev. Lett.* **96** 152501

[16] George S *et al* 2007 Ramsey method of separated oscillatory fields for high-precision Penning trap mass spectrometry *Phys. Rev. Lett.* **98** 162501

[17] Thompson J K, Rainville S and Pritchard D E 2004 Cyclotron frequency shifts arising from polarization forces *Nature* **430** 58

[18] Amoretti M *et al* 2002 Production and detection of cold antihydrogen atoms *Nature* **419** 439

[19] Gabrielse G *et al* 2002 Background-free observation of cold antihydrogen with field-ionization analysis of its states *Phys. Rev. Lett.* **89** 213401

[20] Van Dyck R S, Schwinberg P B and Dehmelt H G 1987 New high-precision comparison of electron and positron g factors *Phys. Rev. Lett.* **59** 26–9

[21] Stahl S, Galve F, Alonso J, Djekić S, Quint W, Valenzuela T, Verdú J, Vogel M and Werth G 2005 A planar Penning trap *Eur. Phys. J.* E **32** 139–46

[22] Galve F, Fernández P and Werth G 2006 Operation of a planar Penning trap *Eur. Phys. J.* D **40** 201–4

[23] Castrejón-Pita J R and Thompson R C 2005 Proposal for a planar Penning ion trap *Phys. Rev.* A **72** 013405

[24] Quint W, Alonso J, Djekić S, Kluge H-J, Stahl S, Valenzuela T, Verdú J, Vogel M and Werth G 2004 Continuous Stern–Gerlach effect and the magnetic moment of the antiproton *Nucl. Instrum. Methods* B **214** 207–10

[25] Verdú J L *et al* 2005 Penning trap measurement of the magnetic moment of the antiproton *AIP Conf. Proc.* **796** 260

[26] Hermanspahn N, Häffner H, Kluge H-J, Quint W, Stahl S, Verdú J and Werth G 2000 Observation of the continuous Stern–Gerlach effect on an electron bound in an atomic ion *Phys. Rev. Lett.* **84** 427–30
[27] Dehmelt H G 1986 Continuous Stern–Gerlach effect: principle and idealized apparatus *Proc. Natl Acad. Sci. USA* **83** 2291–4
[28] Stahl S, Alonso J, Djekić S, Kluge H-J, Quint W, Verdú J and Vogel M 2005 Phase-sensitive measurement of trapped particle motions *J. Phys. B: At. Mol. Opt. Phys.* **38** 297–304
[29] Morse P M and Feshbach H 1953 *Methods of Theoretical Physics* (New York: McGraw-Hill)
[30] Moon P and Spencer D E 1971 *Field Theory Handbook: Including Coordinate Systems, Differential Equations and Their Solutions* (Berlin: Springer)
[31] Jackson J D 2005 *Classical Electrodynamics* (New York: Wiley)
[32] Cohl H C, Tohline J E, Rau A R P and Srivastava H M 2000 Developments in determining the gravitational potential using toroidal functions *Astron. Nachr.* **321** 363–73
[33] Gabrielse G, Haarsma L and Rolston S L 1989 Open-endcap Penning traps for high precision experiments *Int. J. Mass Spectrom. Ion Process.* **88** 319–32
[34] Verdú J 2004 *PhD Thesis* Johannes Gutenberg Universität, Mainz, Germany
[35] Arfken G B and Weber H J 2005 *Mathematical Methods for Physicists* (San Diego, CA: Academic)
[36] Abramowitz M and Stegun I A 1965 *Handbook of Mathematical Functions with Formulas, Graphs, and Mathematical Tables* (New York: Dover)
[37] Cohl H C and Tohline J E 1999 A compact cylindrical green's function expansion for the solution of potential problems *Astrophys. J.* **527** 86–101
[38] Van Dyck R S, Wineland D J, Ekstrom P A and Dehmelt H G 1976 High mass resolution with a new variable anharmonicity Penning trap *Appl. Phys. Lett.* **28** 446
[39] Gabrielse G 1983 Relaxation calculation of the electrostatic properties of compensated Penning traps with hyperbolic electrodes *Phys. Rev.* A **27** 2277–90
[40] Brown L S and Gabrielse G 1986 Geonium theory: physics of a single electron or ion in a Penning trap *Rev. Mod. Phys.* **58** 233–311
[41] Blaum K *et al* 2005 Isoltrap mass measurements of exotic nuclides at $\delta m/m = 10^{-8}$ *Nucl. Phys.* A **752** 317c–20c
[42] Lindell I V 1981 On the 'quasi'-TEM modes in inhomogeneous multiconductor transmission lines *IEEE Trans. Microw. Theory Tech.* **29** 812
[43] Wallraff A, Schuster D I, Blais A, Frunzio L, Huang R-S, Majer J, Kumar S, Girvin S M and Schoelkopf R J 2004 Strong coupling of a single photon to a superconducting qubit using circuit quantum electrodynamics *Nature* **431** 162
[44] Verdú J *et al* 2008 Strong magnetic coupling of an ultracold gas to a superconducting waveguide cavity arXiv:0809.2552v1 [cond-mat.mes-hall]
[45] André A, DeMille D, Doyle J M, Lukin M D, Rabl P, Schoelkopf R J and Zoller P 2006 A coherent all-electrical interface between polar molecules and mesoscopic superconducting resonators *Nat. Phys.* **2** 636
[46] Rabl P, DeMille D, Doyle J M, Lukin M D, Schoelkopf R J and Zoller P 2006 Hybrid quantum processors: molecular ensembles as quantum memory for solid state circuits *Phys. Rev. Lett.* **97** 033003
[47] Pozar D M 2004 *Microwave Engineering* (New York: Wiley)
[48] Simons R N and Arora R K 1982 Coupled slot line field components *IEEE Trans. Microw. Theory Tech.* **30** 1094
[49] Cohn S B 1972 Slot line field components *IEEE Trans. Microw. Theory Tech.* **20** 172